

ML-Driven Optimisation of Luneburg Lens Design

Ravi Kumar Arya[#], Maxon Okramcha^{1,*}, Anant Rajput[§], K.M. Mohan[§], Aditya Sharma[§],
Amitanshu Raj Neti[§], Priyanshu Ganwani[§], Maifuz Ali[~] and Ashwani Kumar[%]

[#]Xiangshan Laboratory, Zhongshan Institute of Changchun University of Science and Technology,
Zhongshan, Guangdong – 528 400, China

¹School of Physics, Changchun University of Science and Technology, Changchun – 130022, China

[§]School of Engineering, Jawaharlal Nehru University, New Delhi - 110 067, India

[~]Electronics and Communication Engineering, IIIT Narya Raipur, Chhattisgarh – 493 661, India

[%]School of Engineering, University of Delhi, New Delhi - 110 007 India

*E-mail: maxonokram8@gmail.com

ABSTRACT

Designing the properties of constant index shells in Luneburg lenses presents a significant challenge due to the inherent mathematical complexity. Although various methods have been proposed to address this issue, many are either overly complex or computationally intensive. However, recent machine learning (ML) advancements have revolutionized solutions to such engineering challenges. This study showcases how ML can streamline the design process for multishell Luneburg lenses, drastically reducing the required effort and computational resources. Our approach employs k-means clustering to determine the properties of the lens's shells. To validate the effectiveness and reliability of our method, we compare simulated results with experimental measurements, demonstrating its accuracy and robustness.

Keywords: Luneburg lens antenna; X-band, Clustering algorithms; K-means; GRIN (Graded Index); ML (Machine Learning); Microwave engineering; Additive manufacturing

NOMENCLATURE

ϵ_r	: Relative permittivity
r	: Radial distance from the centre of the lens
R	: Outer radius
ϵ_1	: Permittivity of air
V_1	: Volume of air void inside the unit cell
$\epsilon_{2,7}$: Permittivity of PLA
$V_{2,7}$: Remaining PLA volume after subtracting V_1 from total volume

1. INTRODUCTION

Relentless pursuit of innovation and discovery has always been a cornerstone of human progress, driving the evolution of technology and society. In the modern era, as the world becomes increasingly interconnected, innovation in communication systems takes centre stage. Antennas, the backbone of modern telecommunications, have seen transformative advancements as engineers strive to achieve higher efficiency, greater range, and precise control of electromagnetic waves. Among the countless challenges in antenna design, the investigation for high gain and directional control stands out as critical, particularly in satellite communication to radar systems and even wireless networks, where antennas must deliver high gain, wide bandwidth, extensive beam scanning capabilities, and strong resistance to interference to ensure enhanced signal

reception¹⁻³. These antennas focus electromagnetic energy into narrow beams, enabling signals to travel over vast distances with minimal loss. Beam scanning or multi-beam antennas further enhance performance by increasing beam coverage. However, achieving such performance has traditionally relied on mechanical steering mechanisms or complex phased arrays—solutions that, while effective, are often bulky, costly, and difficult to maintain.

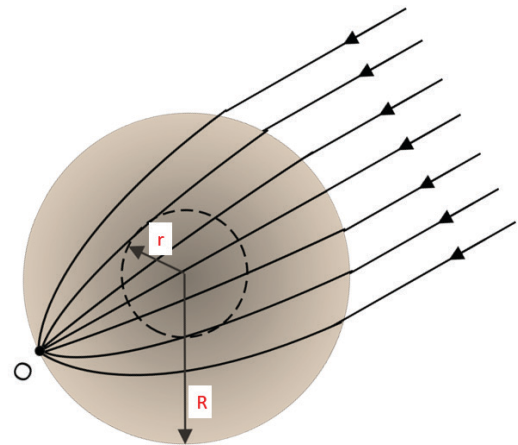


Figure 1. Luneburg lens principle.

This need for simplicity, efficiency, and precision has led researchers to explore alternative solutions to minimize mechanical complexity. While there are various antennas, lens antennas are particularly notable for their excellent performance

in beam steering, focusing, and multi-directional coverage⁴. Unlike conventional high-gain antennas that depend on arrays or reflectors, the Luneburg lens offers an ingenious approach: focusing electromagnetic waves solely through manipulating its refractive index. It is a spherical gradient-index (GRIN) lens⁵ characterized by a radially varying permittivity that decreases from the centre to the outer surface, which R.K. Luneburg first proposed in 1944⁶⁻⁷, based on geometric optics theory. An ideal Luneburg lens can focus electromagnetic waves of a specific wavelength from any incident direction to a precise point on its surface, and vice versa (see Fig. 1). This unique capability allows Luneburg lens antennas to simultaneously receive signals from multiple satellites, making them highly effective for satellite communication applications⁸. Compared to parabolic antennas, they offer notable benefits, including broad frequency bandwidth, easy installation, and strong wind resistance, apart from the capability of electronic scanning. Moreover, compared to expensive phased array antennas⁹⁻¹⁰ that are prone to damage in harsh environments, the Luneburg lens provides the benefits of low cost and stability, making it an ideal choice for mass production in commercial applications.

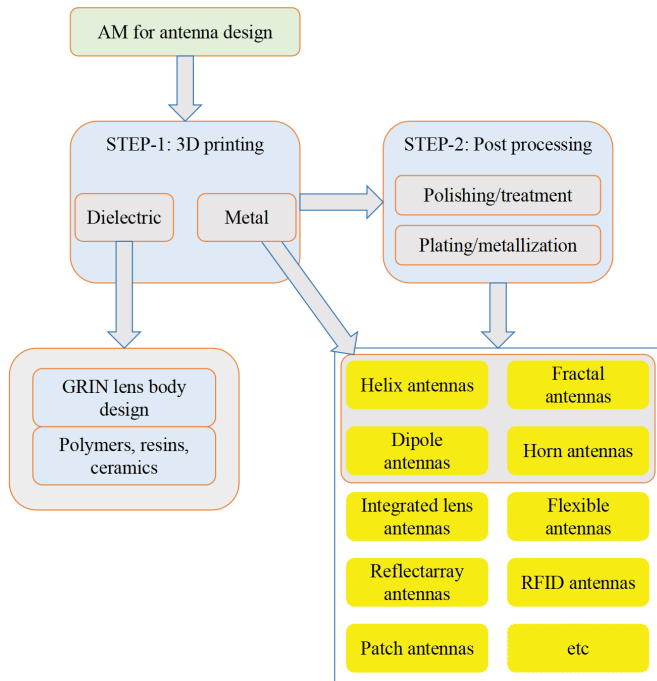


Figure 2. Additive manufacturing for antenna design.

Traditionally, Luneburg lenses have been constructed using a series of concentric inhomogeneous dielectric shells, where the dielectric permittivity is varied in discrete steps^{7,11}. However, this discrete variation often results in less-than-optimal performance as compared to lenses with a continuous permittivity gradient. To address this issue, design optimisation techniques have been developed for multishell Luneburg lenses (LLs) to approximate the continuous gradient by using an optimized finite number of shells¹². While this approach enhances performance, it involves complex mathematical modelling to determine the required permittivity profile for each shell, making the manufacturing process both intricate and time-intensive. For certain GRIN lens designs, the desired

gradient index distribution can be achieved by perforating solid dielectric materials¹³⁻¹⁵. Milling air voids into solid dielectrics alters the effective permittivity. This technique demands the high precision associated with milling to achieve the intended refractive index distribution^{13,16}. A GRIN lens constructed from stacked dielectric sheets with perforated air voids was demonstrated¹⁷. Historically, GRIN lenses were fabricated using natural or engineered materials with specific dielectric properties, typically through laborious subtractive methods like milling. The advent of additive manufacturing (AM) has revolutionised their design and fabrication, enhancing precision, reducing complexity, and broadening their application in wireless communication.

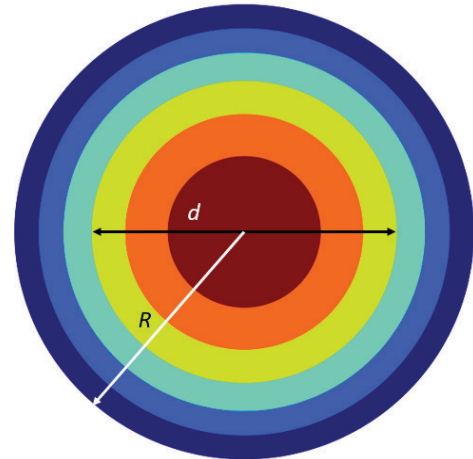


Figure 3. Multishell luneburg lens.

3D printing offers a promising solution for modern antenna design, enabling the creation of intricate geometric profiles while significantly reducing production time and cost. With many 3D printing methods already achieving high resolution, further advancements in additive manufacturing are anticipated. The process of antenna fabrication using additive manufacturing (AM) can be broken into two main steps. The first step involves printing the component (see Fig. 2 [18]). A wide range of materials, including dielectrics and metals, is available for 3D printing. For various types of antennas, a second step is often necessary. This second step may involve post-processing, such as surface polishing or treatment of the printed part and/or plating or metal deposition. Post-processing steps, such as polishing, can alter the dimensions of the printed object. This factor is particularly critical to account for in millimeter-wave and terahertz applications.

To improve the multishell Luneburg lens design process, this work employs machine learning (ML) algorithms to optimize the design, making it more accessible, less computationally demanding, and minimizing the need for complex mathematical calculations, as discussed in Section 2. A comparative analysis is performed between lenses designed using the proposed method and those from prior studies. The lens performance is also evaluated based on its electromagnetic properties in CST Studio Suite, focusing on gain values. The results show a strong agreement with previous findings while achieving faster results with lower computational requirements. Furthermore, the proposed lens is fabricated using 3D printing and measured in Section 3.

2. LUNEBURG LENS DESIGN

A typical spherical Luneburg lens¹⁹ exhibits a spatially varying permittivity profile defined by:

$$\epsilon_r = 2 - \left(\frac{r}{R}\right)^2 \quad (1)$$

where, r represents the radial distance from the centre of the lens, and R denotes the outer radius (see Fig. 1).

Although the mathematical model described by Eqn. (1) suggests that the material properties required for the lens are feasible, in practice, finding materials that naturally exhibit such precise permittivity gradients is challenging. Even when discretizing the lens into multiple concentric spherical shells, as proposed by¹¹⁻¹², it is not feasible to source all the materials commercially off-the-shelf that exactly match the specified permittivity values for each shell. To facilitate practical manufacturing, researchers often reduce the number of shells and optimize the properties of the available materials to approximate the desired permittivity profile. For a Luneburg lens discretized into six shells, the specific thicknesses and relative permittivities for each shell are provided in Table 1 with more details discussed next.

2.1 Design Method Using ML

With the advent of Machine Learning (ML) and advanced computational techniques, the design and optimisation of Luneburg lenses are possible. ML, particularly clustering algorithms, is used in this work for the optimisation of such lenses. Clustering algorithms are unsupervised learning techniques used to group similar data points based on specific characteristics. In the context of Luneburg lens design, clustering algorithms can be employed to discretize the continuous permittivity profile into distinct layers or shells, each with a uniform permittivity. This approach not only simplifies the lens structure but also enhances manufacturability, particularly when designing lenses with a finite number of shells, such as a six-shell Luneburg lens¹¹⁻¹².

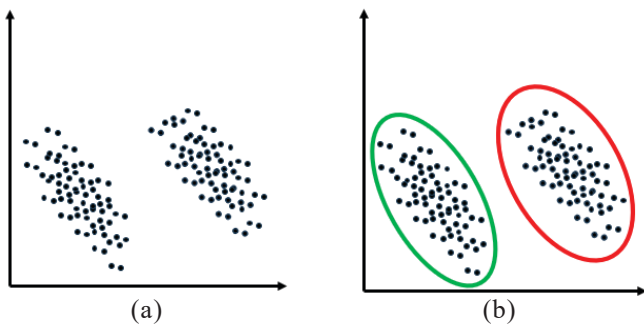


Figure 4. Principle of k-means clustering.

The application of clustering algorithms in designing multi-shell Luneburg lenses involves several steps. First, the continuous permittivity profile of the ideal Luneburg lens is computed. Next, the clustering algorithm is applied to group regions of similar permittivity values, resulting in a set of discrete shells, each corresponding to a shell with a constant permittivity. This process is crucial for translating the theoretical design into a practical, manufacturable lens. The number of shells can be adjusted based on the desired performance and fabrication constraints, with a six-shell design being a popular choice for balancing simplicity and performance¹¹.

There are several clustering techniques out of which, k-means clustering²⁰⁻²¹ is a method of vector quantization that aims to partition n observations into k clusters in which each observation belongs to the cluster with the nearest mean (cluster centroid), serving as a prototype of the cluster. Figure 4 shows how k-means can cluster data into 2 distinct groups.

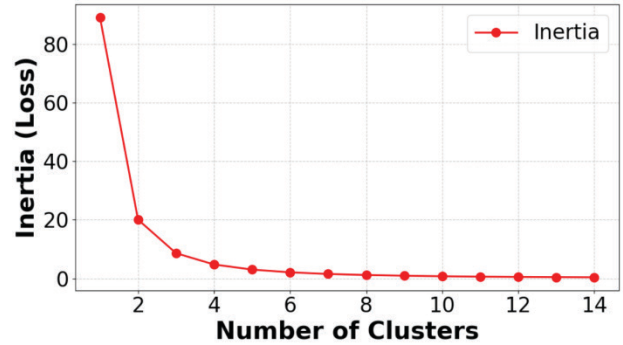


Figure 5. Effect of the number of clusters.

Table 1. Lens properties

Shell No.	Reference lens #1		Reference lens #2		Proposed lens	
	diameter (mm)	ϵ_r	diameter (mm)	ϵ_r	diameter (mm)	ϵ_r
1	39	1.93	31.4	2	33	1.96
2	56	1.77	53.5	1.8	51	1.82
3	68	1.61	69.8	1.6	66	1.65
4	78	1.46	76.9	1.4	79	1.47
5	88	1.31	89.3	1.2	90	1.29
6	96	1.16	95.9	1.08	100	1.10

The drawback of k -means clustering is that just running the model makes it difficult to know how many clusters are needed. For this, it is important to run the different values of clusters and then decide which value to choose. This decision can be made by using the elbow method²². The elbow method helps to find the optimal value of the number of clusters. By looking at Fig. 5, it can be seen that 6 clusters seem appropriate and this number also matches with previous research¹¹ and will be helpful for comparison. For the sake of completeness, other ML methods are compared in Table 2.

The comparison between the previous works, reference lens #1 from¹² and reference lens #2 from¹¹, is shown in Table 1. It is evident from the table that all these lenses have similar shell properties.

2.2 Fabrication of the Proposed Luneburg Lens Using 3D Printing Technology

From Table 1, it is evident that we need 6 discrete permittivity values of dielectrics for the fabrication of the lens. However, finding a dielectric material with ϵ_r between approximately 2 and 1.10 for practical application is quite challenging. Most commercially available dielectric materials

typically have permittivities either higher than 2 (e.g., ceramics, polymers) or close to 1 (e.g., foam), but materials with values precisely between 1.96 and 1.10, as mentioned in Table I, are uncommon. Creating custom materials with these exact permittivity values would require specialised manufacturing, which can be costly and impractical.

Table 2. Comparison of ML models

Shell No.	<i>k</i> -means		Hierarchy		GMM	
	D (mm)	ϵ_r	D (mm)	ϵ_r	D (mm)	ϵ_r
1	33	1.96	27	1.98	20	1.99
2	51	1.82	53	1.83	47	1.88
3	66	1.65	66	1.65	66	1.68
4	79	1.47	78	1.48	79	1.47
5	90	1.29	91	1.28	92	1.27
6	100	1.10	100	1.08	100	1.08

D is the diameter of the particular shell of the lens.

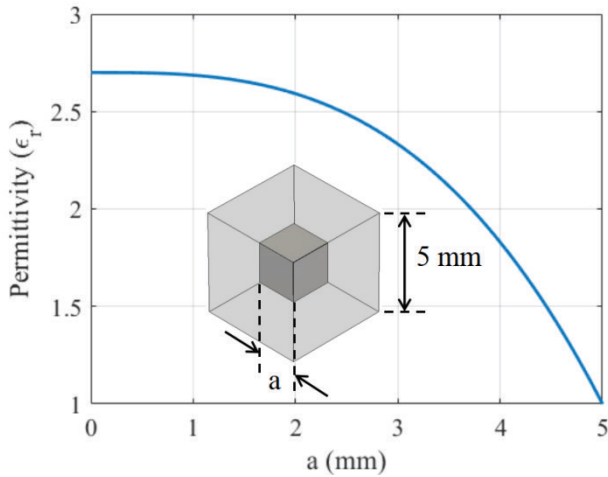


Figure 6. Effective dielectric constant versus air void size.

2.2 Fabrication of the Proposed Luneburg Lens Using 3D Printing Technology

From Table 1, it is evident that we need 6 discrete permittivity values of dielectrics for the fabrication of the lens. However, finding a dielectric material with ϵ_r between approximately 2 and 1.10 for practical application is quite challenging. Most commercially available dielectric materials typically have permittivities either higher than 2 (e.g., ceramics, polymers) or close to 1 (e.g., foam), but materials with values precisely between 1.96 and 1.10, as mentioned in Table I, are uncommon. Creating custom materials with these exact permittivity values would require specialized manufacturing, which can be costly and impractical. However, this once-impossible task becomes feasible with advancements in 3D printing technology. 3D printing allows for the precise fabrication of materials with custom dielectric properties by blending different materials or creating complex structures with varying porosity, making it possible to design and manufacture materials with tailored permittivity values for specific applications.

Table 3. Dimension and relative permittivity of the unit cells

Shell No.	a (mm)	ϵ_r
1	3.79	1.96
2	4.02	1.82
3	4.26	1.65
4	4.49	1.47
5	4.69	1.29
6	4.90	1.10

The material we use for 3D printing is Polylactic Acid (PLA), which has $\epsilon_r = 2.7$ and $\tan \delta$ of 0.01. We introduce a unit cell with an air void to achieve the desired ϵ_r . The unit cell that we use has a dimension of 5 mm × 5 mm × 5 mm (see Fig. 6). The air-void dimension changes w.r.t the desired permittivity. For the lens, the size of the air-void becomes bigger as it moves away from the center, leading to the thinning of the walls on the outside. Figure 6 shows the changes of the ϵ_r w.r.t the change in the size of the air-void. Eqn. (2) is used to plot Fig. 6. The volume of the air void to be placed inside the unit cell is calculated by using Eqn. (2).

$$\frac{(\epsilon_1 \times V_1) + (\epsilon_{2.7} \times V_{2.7})}{\text{Total Volume}} \tag{2}$$

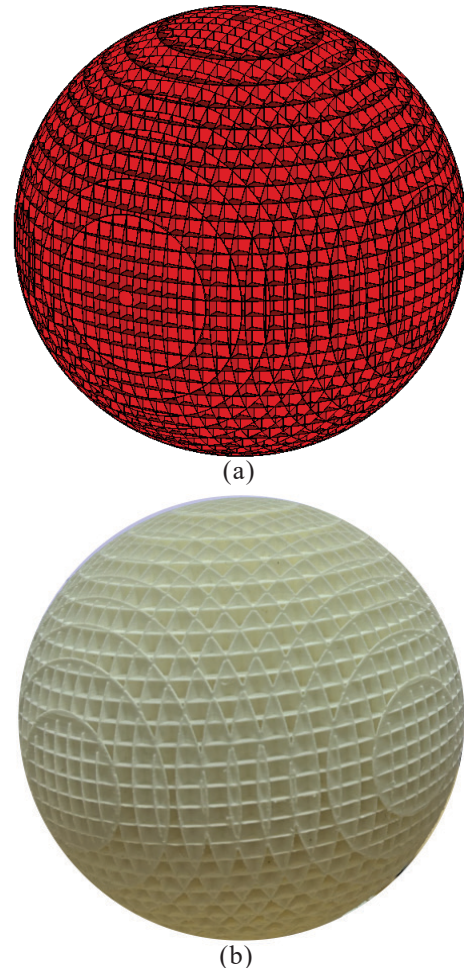


Figure 7. Proposed spherical luneburg lens; (a) Simulated luneburg lens model; and (b) Fabricated prototype luneburg lens.

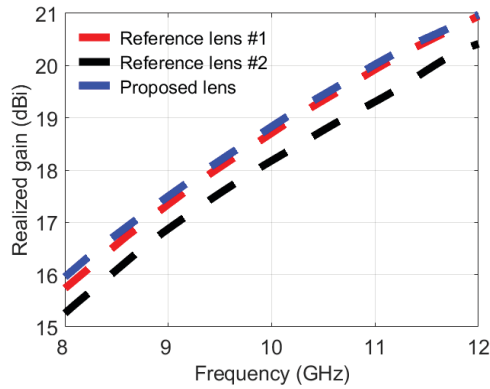


Figure 8. Realised gain comparison.

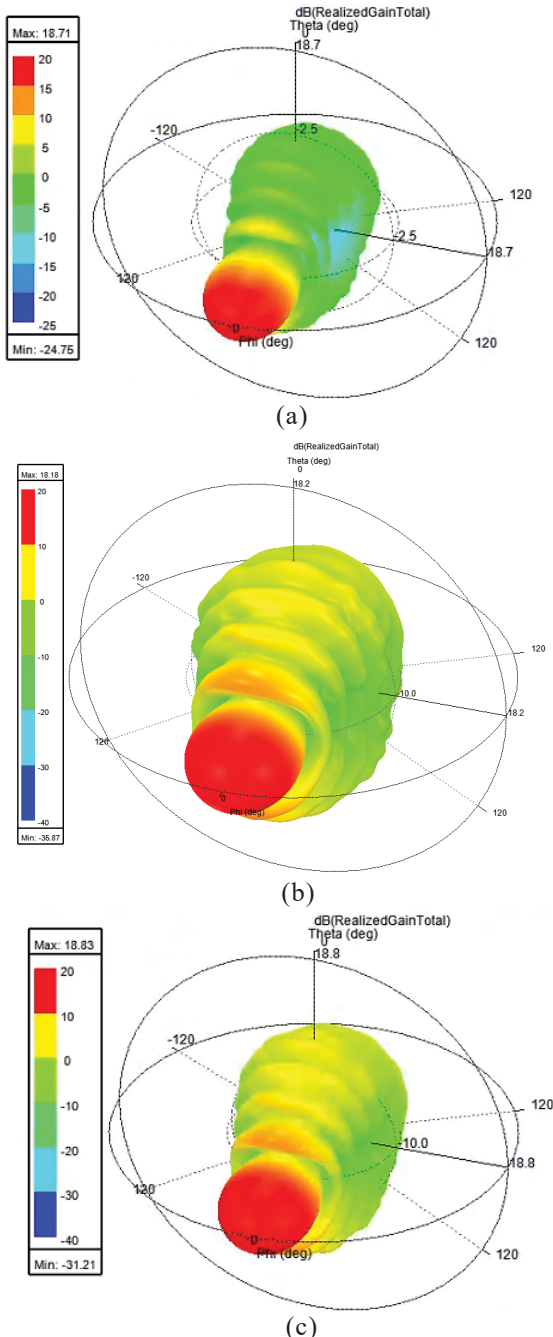


Figure 9. Radiation pattern of luneburg lenses; (a) Reference lens #1; (b) Reference lens #2; and (c) Proposed luneburg lens.

where, ϵ_1 is the permittivity of air, V_1 is the volume of air void, $\epsilon_{2,7}$ is the permittivity of the PLA, and $V_{2,7}$ is the volume that is left after the introduction of void in the unit cell.

We then create six cubes with air voids inside them for each shell. Table 3 shows each air void’s dimension and the unit cell’s relative permittivity. However, the nozzle width of the 3D printer that we have is found to be 0.4 mm, which is bigger than the dimension of the outermost shell, so we only print to the fifth shell. So, we use the 6th shell made of foam. Figure 7 shows the simulated lens of 6 shells and the fabricated lens of 5 inner shells.

3. RESULTS AND DISCUSSION

While simplifying the lens design process with ML methods is straightforward, it is crucial to demonstrate that the proposed method yields a lens with comparable or superior properties compared to prior works. To validate this, we performed electromagnetic simulations using CST Studio Suite to compare the radiation characteristics of the lens designed by the proposed method against those from previous research. Specifically, we designed the lens using the current method, maintaining the same dimensions and operating frequency as those in the prior studies¹¹⁻¹².

For comparison, all three lenses are fed by a waveguide (WR90) working in the 8-12 GHz frequency range. The gain response of these lenses is shown in Fig. 8. The plot shows that the proposed method shows a slight improvement in the results from the reference works (reference lens #1 from¹² and reference lens #2 from¹¹). Fig. 9 shows the 3D radiation patterns of all the lenses. These patterns also look similar, with slight variations in gain values.

Having a similar response of the multishell Luneburg lens from the proposed method to past research works verifies that the proposed method is well suited for designing such lenses due to the reduced effort and computational resources required.

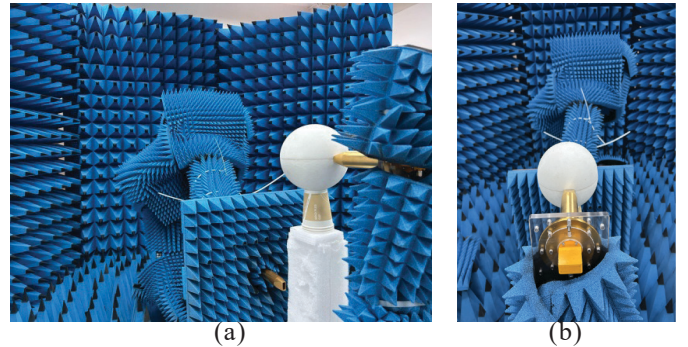


Figure 10. Measurement setup for the proposed lens; (a) Side view; and (b) Top view.

Before concluding this discussion, it is essential to note that several other clustering algorithms were tested, but k-means was the most effective. Its iterative approach and ability to minimize within-cluster variance allowed it to partition the data into well-separated clusters accurately. Hierarchical clustering and Gaussian Mixture Models (GMM) were found to be less precise when compared with the reference lens but had good metric scores. Their simulation results were similar with minute differences. Density-Based Spatial Clustering of Applications with Noise (DBSCAN) struggled because it identified only one

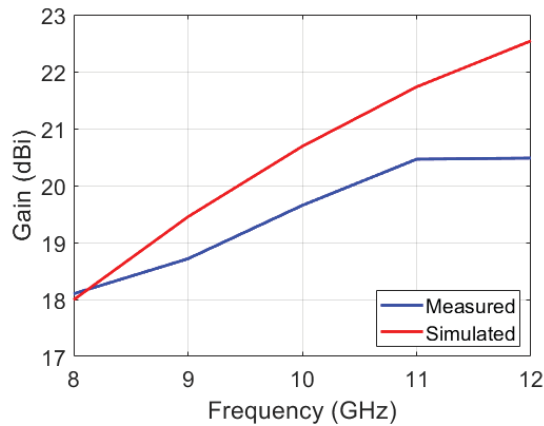


Figure 11. Measured and simulated gain comparison.

cluster due to the data's uniform density and lack of distinct density variations. Affinity Propagation and Mean Shift, which both attempt to determine the number of clusters dynamically, also faced challenges. Affinity Propagation was not well-suited for the dataset's smooth, continuous nature, leading to either excessive or degenerate clusters, while Mean Shift aggregated most data points into a single cluster due to insufficient density variations.

3.1 Measurement of the Proposed Luneburg Lens

The fabrication of the proposed lens took about 173 hours. After the fabrication, the measurement chamber was set up, which uses a planar near-field measurement system. The transmitting waveguide (WR90) and proposed Luneburg lens acted as an antenna under test (AUT), and the receiving waveguide (WR90) was the "Probe". The measurement plane distance between the AUT and probe is 3λ to 5λ of the operating frequency. The scan plane's dimension is 30λ of the highest frequency. The measurement setup is shown in Fig. 10. After the lens measurement, we replaced the AUT with the known X-band horn antenna. The distance between the horn antenna flare and the AUT to the probe should be equal. We then measure the power at $\phi=90^\circ$ for both the AUT and the horn antenna to calculate the gain of the proposed Luneburg lens. We use the gain transfer method to measure the gain of the lens using Eq. 3. Fig. 11 shows the gain comparison between the fabricated lens and the simulated lens.

4. CONCLUSIONS

This study demonstrates how machine learning can simplify the traditionally complex and resource-heavy design process of multishell Luneburg lenses. By leveraging k-means clustering, the proposed method efficiently determines the properties of the lens's shells, reducing both effort and computational demands. The successful validation against measured results underscores the reliability and robustness of this ML-driven approach, opening new possibilities for more efficient lens design workflows.

REFERENCES

1. Che, X.; Gao, J. & Li, Z. 3-D printed high-gain elliptic flat Luneburg lens. *Results in Physics.*, 2024, **57**, 107350.
2. Boccia, L. Amendola; G. & Di Massa, G. A high

- performance dual frequency microstrip antenna for global positioning system. *In IEEE Antennas and Propagation Society International Symposium. 2001 Digest, Held in conjunction with: USNC/URSI National Radio Science Meeting (Cat. No. 01CH37229)*, IEEE, 2001, **4**, 66–69.
3. Wei, K.; Zhang, Z. & Feng, Z. Design of a coplanar integrated microstrip antenna for gps/its applications. *IEEE Antennas and Wireless Propag. Lett.*, 2011, **10**, 458–461.
4. Mittra, R.; Nasri, A. & Arya, R.K. Wide-angle scanning antennas for millimeter-wave 5G applications. *Engin.*, 2022, **11**, 60–71.
5. Zhang, S.; Arya, R.K.; Whittow, W.G.; Cadman, D.; Mittra, R. & Vardaxoglou, J. Ultra-wideband flat metamaterial GRIN lenses assisted with additive manufacturing technique. *IEEE Transact. Antennas and Propag.*, 2020, **69**(7), 3788–3799
6. Luneburg, R.K. *Mathematical theory of optics*. University of California Press, 1966
7. Peeler, G. & Coleman, H. Microwave stepped-index luneburg lenses. *IRE Transact. on Antennas and Propag.*, 1958, **6**(2), 202–207,
8. Thornton, J.; Smith, D.; Foti, S. & Jiang, Y. Reduced height luneburg lens antennas for satellite communications-on-the-move. *In 2015 Conference on Microwave Techniques (COMITE)*. IEEE, 2015, pp.1–4.
9. Wen, Y.Q.; Wang, B.Z. & Ding X. A wide-angle scanning and low sidelobe level microstrip phased array based on genetic algorithm optimisation. *IEEE Transact. on Antennas and Propagat.*, 2015, **64**(2), 805–810.
10. Valavan, S.; Tran, D.; Yarovoy, A. & Roederer, A. Planar dual-band wide-scan phased array in X-band. *IEEE Transact. on Antennas and Propagat.*, 2014, **62**(10), pp. 5370–5375.
11. Mateo-Segura, C.; Dyke, A.H.; Dyke, Haq, S. & Hao, Y. Flat Luneburg lens via transformation optics for directive antenna applications, *IEEE Transact. on Antennas and Propagat.*, 2014, **62**(4), 1945–1953.
12. Fuchs, B.; Coq, L. Le; Lafond, O.S.; Rondineau & Himdi, M. Design optimisation of multishell Luneburg lenses. *IEEE Transact. Antennas and Propag.*, 2007, **55**(2), 283–289.
13. Garcia, N.C. & Chisum, J.D. High-efficiency, wideband grin lenses with intrinsically matched unit cells. *IEEE Transact. on Antennas and Propagat.*, 2020, **68**(8), 5965–5977.
14. He, Y. & Eleftheriades, G.V. Matched, low-loss, and wideband graded-index flat lenses for millimeter-wave applications. *IEEE Transact. on Antennas and Propagat.*, 2018, **66**(3), 1114–1123.
15. Mahmoud, A.E.; Hong, W.; Zhang, Y. & Kishk, A. W-band multilayer perforated dielectric substrate lens. *IEEE Transact. on Antennas and Propagat. Lett.*, 2014, **13**, 734–737.
16. Mei, Z.L.; Bai, J. & Cui, T.J. Gradient index metamaterials realized by drilling hole arrays. *J. Physics D: Appl. Physics*, 2010, **43**(5), 055404
17. Zhang, N.; Jiang, W.X.; Ma, H.F.; Tang, W.X. & Cui,

- T.J. Compact high-performance lens antenna based on impedance-matching gradient-index metamaterials. *IEEE Transact. on Antennas and Propagat.*, 2018, **67**(2), 1323–1328
18. Munina, I.; Grigoriev, I.; O'donnell, G. & Trimble, D. A review of 3D printed gradient refractive index lens antennas. *IEEE Access*, 2023, **11**, 8790–8809.
 19. M. Ansari, B. Jones, and Y. J. Guo, Spherical luneburg lens of layered structure with low anisotropy and low cost. *IEEE Transact. on Antennas and Propagat.*, 2022, **70**(6), 4307–4318.
 20. Burkardt, J. K-means clustering, Virginia Tech, Advanced Research Computing, Interdisciplinary Center for Applied Mathematics, 2009.
 21. Pedregosa, F.; Varoquaux, G.; Gramfort, A.; Michel, V.; Thirion, B.; Grisel, O.; Blondel, M.; Prettenhofer, P.R.; Weiss, V.; Dubourg, J.; Vanderplas, A.; Passos, D.; Cournapeau, M.; Brucher, M.P. & Duchesnay, E. Scikit-learn: Machine learning in python. *J. Mach. Learn. Res.*, 2011, **12**, 2825–2830.
 22. Cui, M. Introduction to the k-means clustering algorithm based on the elbow method. *Account. Audit. and Financ.*, 2020, **1**(1), 5–8.

CONTRIBUTORS

Dr Ravi Kumar Arya obtained his PhD from Pennsylvania State University (USA). He is currently with the Zhongshan Institute of Changchun University of Science and Technology. His research focuses on electromagnetic theory, antenna engineering, computational electromagnetics, and AI applications. Contribution in the current study: He conceived the study, designed the research framework, and supervised all project stages, including methodology development, data analysis, and manuscript preparation.

Mr Maxon Okramcha obtained his MTech from Amity University, Noida. Currently, he is a PhD student at Changchun University of Science and Technology, based at the Xiangshan Laboratory, Zhongshan Institute of Changchun University of Science and Technology. His research focuses on computational electromagnetics, antenna engineering, RF fabrication, RF measurement, and microwave engineering. In the current study he conducted lens simulations, fabrication, and measurements, and drafted the initial manuscript.

Mr Anant Rajput is a BTech CSE student at Jawaharlal Nehru University. His areas of interest include: Machine learning, deep learning, and data analytics. Skilled in Python, PyTorch, and TensorFlow. He worked on predictive modeling, computer vision, and big data projects. He is passionate about data-driven solutions and research.

For this study, he designed and performed the simulations, validated the results, and contributed to manuscript revisions.

Mr K.M. Mohan is a BTech ECE student at Jawaharlal Nehru University. His areas of interest include: Antennas, electromagnetics, RFIC, and IoT. He is proficient in HFSS, ADS, CST, Python, and MATLAB, with hands-on experience in IoT-based automation projects. He is actively engaged in research and tech innovation.

For this study, he performed the simulations and contributed to manuscript revisions.

Mr Aditya Sharma is a BTech CSE student at Jawaharlal Nehru University. His areas of interest include: Computer architecture, computer vision, and high-performance simulation software. He is skilled in Graph Neural Networks, TensorFlow, Qt, wxWidgets, and OpenCascade for CAD development.

For this study, he performed the simulations and contributed to manuscript revisions.

Mr Amitansu Raj Neti is a MTech student at Jawaharlal Nehru University's School of Engineering. His areas of interest include: Software engineering and computational technologies. He is passionate about performance optimisation and graphics programming.

For this study, he performed the simulations and contributed to manuscript revisions.

Mr Priyanshu Ganwani is pursuing a dual degree at Jawaharlal Nehru University. His areas of interest include: Computer vision, deep learning, and machine learning. His research focuses on advancing these technologies to solve complex real-world problems.

For this study, he performed the simulations and contributed to manuscript revisions.

Dr Maifuz Ali obtained PhD from IIT Kharagpur and working as an Associate Professor in Electronics and Communication Engineering at IIIT-NR. His research focuses on electromagnetics, scattering, ray tracing, channel modeling, EMI sensors, RCS, millimeter waves, bioelectromagnetics, and non-reciprocal devices. Contribution in the current study: He supervised the study, drafted sections of the manuscript, and revised the final version.

Dr Ashwani Kumar obtained his PhD in Electronics from the University of Delhi South Campus. He was a Post-Doctoral Researcher at the University of Central Florida. He is working as an Associate Professor at the University of Delhi South Campus. His research focuses on microwave passive components, including filters, MIMO/UWB antennas, and metamaterial-based designs.

He supervised the study, drafted sections of the manuscript, and revised the final version.